

Heat transfer characterization of plate fin-tube heat exchangers

N. Kayansayan

Dokuz Eylül University, Department of Mechanical Engineering, Bornova 35100, Izmir, Turkey

Received 5 March 1992; revised 13 October 1992

The effects upon the performance of plate fin-tube cross flow heat exchangers due to outer surface geometry are considered. The finning parameter varying from 11 to 23, a total of 10 geometrically distinct configurations was tested over a Reynolds number range from 100 to 30 000. The tube outside diameter with the collar thickness defines the characteristic dimension. The convective heat transfer coefficients are presented as plots of Colburn j -factor versus Reynolds number and compare well with previous studies. The dispersion in the majority of data is $\pm 10\%$. The j -factor, the Reynolds number and the finning parameter are correlated.

(Keywords: heat transfer; heat exchanger; plate exchanger; plate-fin; Reynolds; geometry; measurement; test)

Caractérisation du transfert de chaleur d'échangeurs de chaleur à plaques-ailettes

On considère l'efficacité d'échangeurs de chaleur à écoulements croisés et à plaques-ailettes, en fonction de la géométrie de la surface extérieure. Le paramètre d'ailetage variant de 11 à 23, on a testé dix configurations géométriquement différentes, pour des nombres de Reynolds compris entre 100 et 30 000. Le diamètre extérieur du tube et l'épaisseur de l'ouverture définissent une dimension caractéristique. On présente les coefficients de transfert de chaleur par convection sous la forme de diagrammes où le coefficient j de Colburn est porté en fonction du nombre de Reynolds. Les résultats sont en bonne cohérence avec les études précédentes. La dispersion des données est en général de plus ou moins 10%. On corrèle le coefficient j , le nombre de Reynolds et les paramètres des ailettes.

(Mots clés: transfert de chaleur; échangeur de chaleur; échangeur à plaque; plaque-ailette; Reynolds; géométrie; mesure; essai)

Plate fin-tube heat exchangers are quite common in applications related to the air conditioning, heating and refrigeration industries. Due to the complex pattern of the fluid flow over the fin-and-tube surface, the theoretical prediction of heat transfer coefficients is often precluded. The combined process of heat and momentum transfer serves to complicate the analysis. Therefore, it is necessary to resort to experimentation in order to construct useful models.

A variety of flow configuration have been studied and documented in the literature. Reviews of the literature have been given by Webb¹ and McQuiston². The results reported here, however, are unique in that the present study not only extends the range of the geometrical parameters of previous studies but also considers a larger Reynolds number range. This review is not intended to be exhaustive, but rather to provide a background for the present study.

Rich^{3,4} examined the effects of fin spacing and the number of tube rows on the heat transport of several heat exchangers. Varying the number of tube rows from one to six, Rich concluded that, depending upon the Reynolds number, the average heat transfer coefficients for a deep coil may be higher or lower than that for a shallow coil.

In the Colburn j -factor correlation stated by Elmahdy and Biggs⁵, the Reynolds number exponent, m , was assumed to be a strong function of the physical parameters of the finned tube exchanger over the Reynolds

number range from 200 to 2000. Experiments were performed, and the m values for every individual exchanger with specified geometry were determined by a regression analysis method.

McQuiston⁶ developed a very simple correlation for four-row staggered banks with plain fins. It was found that the j -factors were best correlated by applying a multiplication factor to the Reynolds number given by $(A_o/A_{io})^n$. The Reynolds number in the analysis ranged between 100 and 4000.

The work now presented documents the average heat transfer coefficients for 10 distinct fin-tube-bank configurations obtained from controlled experiments in a wind tunnel. In the experiments, the number of tube rows along the flow direction was four, and the Reynolds number was spanned in the range from 10^2 to 3×10^4 . The characteristic dimension, containing the collar wall thickness, is the tube outside diameter. This choice enables correlating the heat transfer data in a compact form. Comparison of the present results with previous studies is also provided.

Experimental setup and instrumentation

The wind tunnel

A wind tunnel facility, similar to the one used in previous compact exchanger analysis⁷, was modified to accept exchanger prototypes with approximately 0.25 m² fron-

Nomenclature			
A	Surface area, m^2	n	Number of tubes per row
B	The exchanger height, m	s_F	Fin density, fins m^{-1}
E	Percentage of error (Equation (14)), dimensionless	s	Fin spacing, m
F	Correction to logarithmic temperature difference, dimensionless	s_1	Transverse tube pitch, m
G_m	The mass flux, $kg\ m^{-2}\ s^{-1}$	s_2	Longitudinal tube pitch, m
H	Air-side enthalpy, W	t	Fin thickness, m
L	The flow length, m	t_c	Collar thickness, m
M	Mass flow rate, $kg\ s^{-1}$	<i>Greek letters</i>	
N	Number of tube rows	Δ	Difference
Nu	Nusselt number, $h_o d_o/k_b$, dimensionless	ϵ	The exchanger finning factor (Equation (6)), dimensionless
Pr	Prandtl number, $\mu_b c_p/k_b$, dimensionless	η	Efficiency
Q	Heat transfer rate, W	μ	Dynamic viscosity, $kg\ m^{-1}\ s^{-1}$
Re	Reynolds number, $G_m d_o/\mu_b$, dimensionless	ρ	Density, $kg\ m^{-3}$
T	Temperature, $^{\circ}C$	σ	Minimum to frontal area ratio, dimensionless
ΔT_m	Logarithmic mean temperature difference, $^{\circ}C$	<i>Subscripts</i>	
U	Overall heat transfer coefficient, $W\ m^{-2}\ ^{\circ}C^{-1}$	b	Bulk
V	Velocity, $m\ s^{-1}$	e	Exit
a	Segmental area of the wind tunnel cross section, m^2	f	Fin
c_p	Specific heat, $kJ\ kg^{-1}\ ^{\circ}C^{-1}$	fr	Frontal
d	Diameter, m	h	Hydraulic
h	Heat transfer coefficient, $W\ m^{-2}\ ^{\circ}C^{-1}$	i	Inside
j	Colburn j -factor, $(h_o/G_m c_p) Pr^{2/3}$, dimensionless	in	Inlet
k	Thermal conductivity, $W\ m^{-1}\ ^{\circ}C^{-1}$	j,k	Measurement points
m	Reynolds number exponent (Equation (4))	min	Minimum
		o	Outside
		to	Tube outside

tal area and to provide two-dimensional flow as free of vibration and turbulence as reasonably possible for exchanger performance studies. A schematic diagram of the wind tunnel is shown in *Figure 1*. The system is designed to suck room air over the finned side of the exchanger while circulating hot water through the tubes. The tunnel, made of 0.5 mm thick galvanized sheet metal, was a square duct of 50 cm \times 50 cm in cross section and 1100 cm in overall length. To avoid the flow of dust particles into the system, the entrance section contains two 100 cm \times 100 cm screens of 10 meshes per cm, and 0.2 mm diameter steel wire cloth. Through a 50 cm long Zanker type flow straightener⁸, air flows approximately 500 cm in a straight horizontal duct before reaching the test section. As depicted in *Figure 1*, the duct wall surfaces at 100 cm downstream and upstream of the test section are furnished with a total of 12 holes of 10 mm diameter. Axisymmetric with these holes, cylindrical Teflon elements, having 10 mm inside diameter, are attached to the tunnel to provide access holes for the velocity probe. Air leaving the metering section flows through a sheet metal transition section and enters the fan. At the fan exit, the air is discharged to the surroundings. To minimize the heat losses to the surroundings, the tunnel outer surface is insulated with a 2 cm thick glass wool layer. Additionally, being supported by stands of perforated steel plates, the duct system is elevated 50 cm above floor level of the laboratory room.

Power for the wind tunnel was provided by a Sontec Model 6938 fan driven by a 3 kW AC motor. The motor was in turn powered by an electronic variac (a three-phase motor control unit) and the fan speed could be varied in a continuous manner from 0 to 1350 rpm. Thus it was possible to alter the tunnel air velocity in the range from 0 to 15 $m\ s^{-1}$. A digital display panel indicated the fan rotational speed.

The hot water system

The hot water system consists of a boiler of 115 kW heating capacity, a circulating pump, a flow metering unit and the test exchanger. All components of the system were interconnected through 25 mm in diameter insulated steel piping. Thus, a closed circuit between the boiler and the test exchanger was established. The boiler contained 1500 l of water and was fired by a burner. A Honeywell thermostat, located at the exit, kept the water temperature at a preset value of 80 $^{\circ}C$. The burner was controlled by the thermostat so that the exit water temperature was allowed to vary within $\pm 3^{\circ}C$ of the preset value. Owing to the large capacity of the boiler tank, stable temperatures at the exit were achieved.

The test heat exchanger

Figure 2 shows the fin layout and the tube circuit arrangement of the exchanger that was studied in this

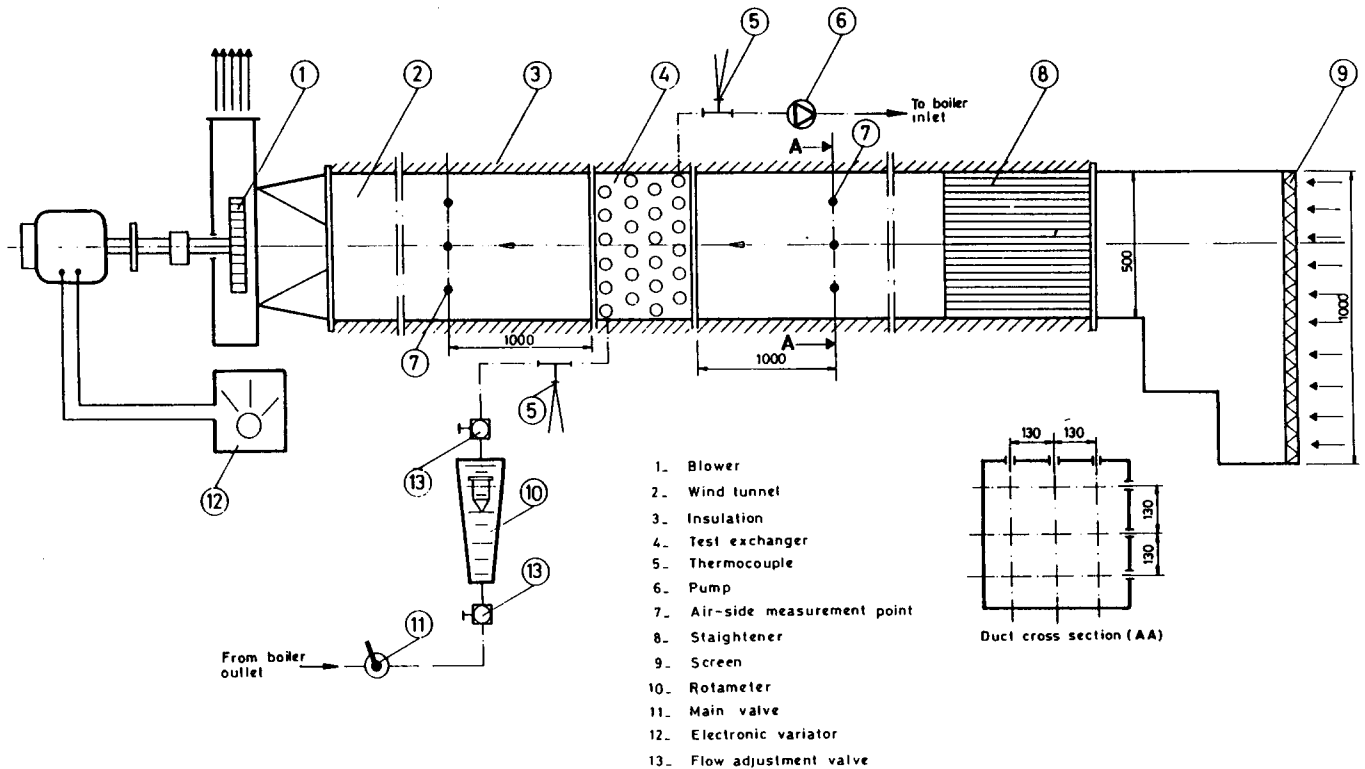


Figure 1 A schematic diagram of the experimental apparatus and the instrumentation
 Figure 1 Schéma de l'appareil expérimental et des instruments

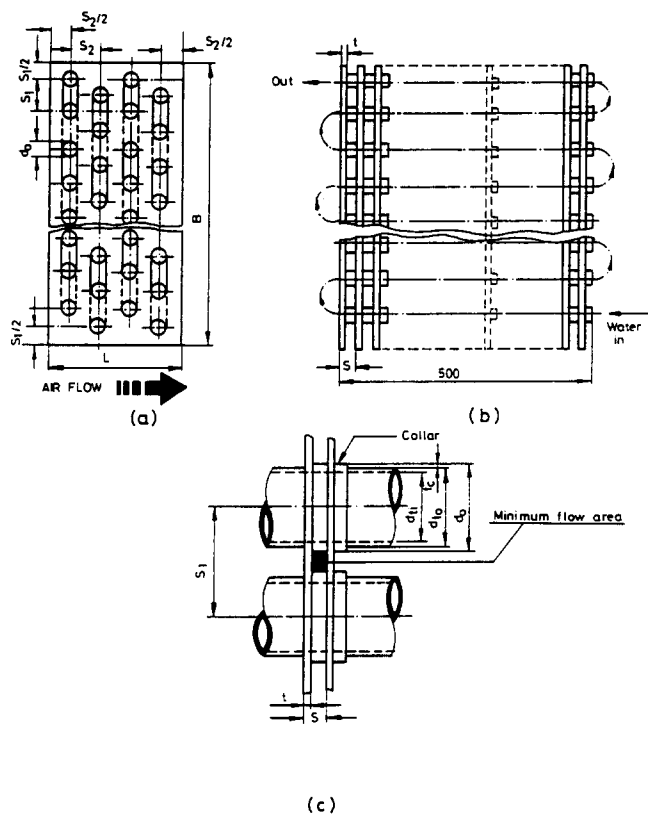


Figure 2 (a) The heat exchanger characteristic geometry. (b) The multipass water flow circuit. (c) The magnified view of the tube-fin combination
 Figure 2 (a) Géométrie de l'échangeur de chaleur; (b) circuit d'écoulement de l'eau à passages multiples; (c) schéma de la combinaison tube-ailette

experiment. *Table 1* presents the geometrical parameters of all the tested coils. Each core had flat, continuous 0.2 mm thick aluminium fins with collars. The copper tubes of 0.5 mm wall thickness, a product of Wieland Corporation, were manufactured with ± 0.06 mm tolerance on the outside diameter (o.d.). After the assembly, the tubes were mechanically expanded into the fins and tube sheets. The mechanical bond between the fins and tubes was checked and judged to be quite tight, and a negligible fin-tube thermal contact resistance was secured. The return bends were manually soldered to the tube extensions. Thus, the tubes of each row were interconnected, and four identical, multipass cross flow circuits connected in parallel were obtained. Avoiding any possible clogging, each circuit was tested by pressurized air. Then, the 25 mm steel tubing headers for the supply and the collection of hot water through the circuits were attached. The tube sheets which form a casing for the core and possess mounting holes on its periphery were fabricated of galvanized steel sheet 0.5 mm in thickness.

Instrumentation

The hot water supply to the test section was metered by an ASA glass tube variable area rotameter. The meter had a sensitivity of 1 l min^{-1} per cm of the bob displacement and was calibrated to be accurate within $\pm 2\%$ of the full range. The flow rate adjustment through the coil was accomplished by two gate valves located at the inlet and the outlet of the rotameter.

The water temperatures were recorded by a Sonde temperature indicator set. Measuring temperatures in the range of -15°C to $+90^\circ\text{C}$, the probes of the instrument were 24 AWG copper-constantan (Type T) thermocouple elements enclosed in a 10 mm o.d. stainless steel

Table 1 Geometric parameters of the tested coils
 Tableau 1 Paramètres géométriques des batteries essayées

Coil type	Tube diameter d_o (mm)	Coil height B (mm)	Flow length L (mm)	Transverse pitch s_1 (mm)	Longitudinal pitch s_2 (mm)	Fins per m s_F (m^{-1})	Exchanger finning factor ϵ	Tubes per row n	Number of rows N
1	16.3	500	139	40	34.67	454	23.24	12	4
2	16.3	500	139	40	34.67	312	15.81	12	4
3	16.3	500	139	40	34.67	238	12.12	12	4
4	9.52	480	104	30	26	454	23.53	16	4
5	9.52	480	104	30	26	312	16.00	16	4
6	9.52	480	104	30	26	238	12.33	16	4
7	9.52	482	88	25.4	22	454	16.44	19	4
8	9.52	482	88	25.4	22	312	11.28	19	4
9	9.52	482	88	25.4	22	400	14.43	19	4
10	12.5	493	127	31.75	32	454	22.81	15	4

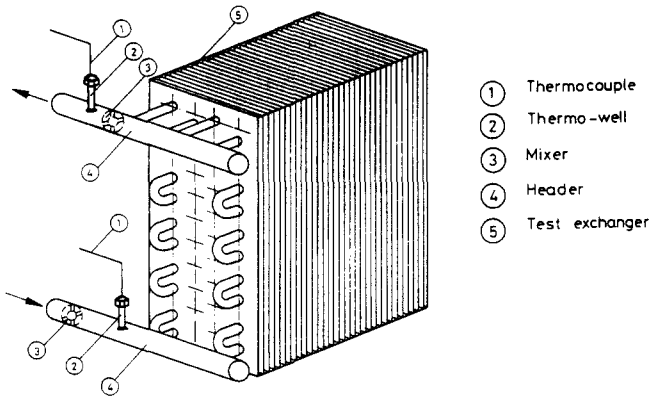


Figure 3 A schematic diagram of the water-side flow distribution and the instrumentation
 Figure 3 Schéma latéral de la circulation de l'eau et de l'instrumentation

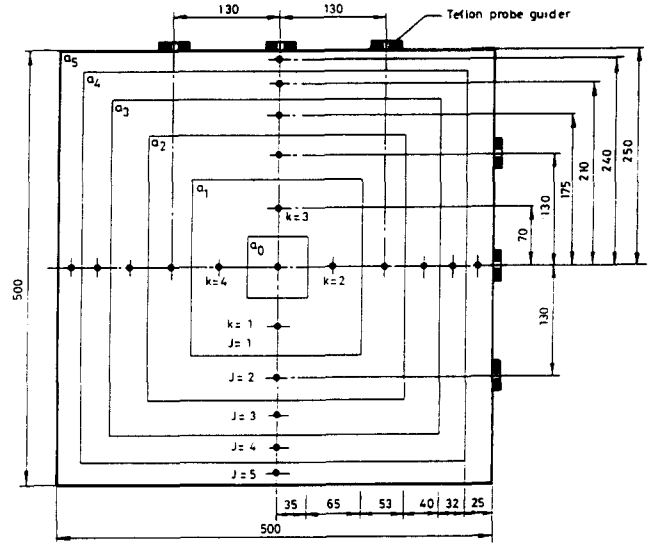


Figure 4 The wind tunnel cross section illustrating the velocity and the temperature measurement points
 Figure 4 Coupe du tunnel aéronautique illustrant la vitesse et les points de mesure de la température

protection tube. Vinyl-insulated lead wires terminated at the socket junction of the analogue indicator. The set was calibrated by placing the probes in a variable-temperature bath whose temperature was measured by a precision thermometer. As illustrated in Figure 3, the probes were housed in wells of the exchanger headers and their positions were fixed by fittings. To attain uniform water temperatures, two mixers, made of perforated shims, were located upstream of both probes.

The air stream velocity and temperature measurements were obtained by a TSI Model 1650-1 hot-wire, constant-temperature anemometer. The extendable probe wand had a sensing tip of 4.7 mm in diameter. Using the sensor as a resistance thermometer, the instrument was also capable of measuring the air temperatures. As specified by the manufacturer, the accuracy in velocity measurements was $\pm 2\%$, and in temperature measurements $\pm 0.8\%$ of the full scale.

A barometer indicated the ambient pressure, and a psychrometer was used to measure the dry bulb and the wet bulb temperatures of the room air.

Experimental procedure and data reduction

The heat exchanger with specified surface geometry was installed in the wind tunnel in such a manner that the horizontal position was checked by a level, and the tunnel connections were sealed by epoxy. For some configurations, the exchanger height was less than the tunnel dimensions and the bypass flow was eliminated by a thin

layer of foam plastic sandwiched between the edges of fins and the casing. Upon completion of the water-side links, the coil was completely insulated by a 5 cm thick layer of glass-wool. The air in the water circuit was purged out through the purging plugs. The upstream and the downstream valves of the rotameter were adjusted such that the average water velocity through the coil tubes was approximately 0.5 m s^{-1} and then the tunnel blower was turned on, and the air velocity was adjusted to a desired value. The water inlet and outlet temperatures were periodically checked and equilibrium was assumed to exist if no appreciable deviation in water temperature change was observed for the last 15 min prior to data recording.

As shown in Figure 4, the tunnel cross section was divided into six segmental areas, and in accordance with the log-linear rule⁸, the velocity and the temperatures of the air stream at a total of 21 grid points were measured. The air-side mass flow rate was then determined as follows:

$$M = (\rho a V)_o + \frac{1}{4} \sum_{j=1}^5 a_j \sum_{k=1}^4 (\rho_k V_k)_j \tag{1}$$

where the subscript, k , indicates the four velocity values at a particular segmental area a_j .

Table 2 Experimental uncertainties
Tableau 2 Incertitudes expérimentales

Property	Uncertainty	Range
Water flow rate	$\pm 0.5 \text{ l min}^{-1}$	Up to 28 l min^{-1}
Inlet water temperature	$\pm 0.8^\circ\text{C}$	$77\text{--}84^\circ\text{C}$
Water temperature difference	$\pm 1^\circ\text{C}$	$10\text{--}41^\circ\text{C}$
Outlet air temperatures	$\pm 0.8^\circ\text{C}$	$29.2\text{--}67.8^\circ\text{C}$
Inlet air temperatures	$\pm 0.5^\circ\text{C}$	$7\text{--}19.5^\circ\text{C}$
Air velocity	$\pm 0.06 \text{ m s}^{-1}$	$0\text{--}3 \text{ m s}^{-1}$
Air velocity	$\pm 0.2 \text{ m s}^{-1}$	$2.5\text{--}12.5 \text{ m s}^{-1}$
Probe access length	$\pm 1 \text{ mm}$	$25\text{--}475 \text{ mm}$

Similarly, the air enthalpy at the exit is

$$H_e = (\rho a V c_p T)_o + \frac{1}{4} \sum_{j=1}^5 a_j \sum_{k=1}^4 (\rho_k c_{p,k} V_k T_k)_j \quad (2)$$

Due to uniform temperature distributions at the inlet of the test section, the inlet air enthalpy is

$$H_{in} = M c_{p,in} T_{in} \quad (3)$$

The difference between Equations (2) and (3) yields the heat rate gained by air, and was compared with the heat loss of the water. In most experimental runs, the heat rate difference between the two sides was within $\pm 5\%$ range of the water-side heat rate. In calculating the exchanger overall conductance, UA , however, the arithmetic average of the air and the water-side heat rates was taken into account. The uncertainties in the measured properties were estimated to be as in *Table 2*. With the uncertainties given in *Table 2*, and over the indicated ranges, the method of Kline and McClintock⁹ was employed to evaluate the uncertainties of the experimental results. For a typical case, the average heat flow rates were found to be within 6.1%, the Reynolds numbers within 8.1% and the j -factors within 11.2% of the reported values.

By the Colburn analogy¹⁰ the functional relationship, $Nu = \phi(Re, Pr, \text{flow geometry})$, suggested by the governing equations becomes

$$Nu = C Re^m Pr^{1/3} \epsilon^n \quad (4)$$

for Prandtl numbers in the range $0.5 < Pr < 100$. For the test cases, it was calculated that $Pr \sim 0.7$. In this study the maximum velocity, i.e. the velocity at the minimum flow area, was used for the Reynolds number characteristic velocity and as given by Equation (A1) in Appendix A the characteristic diameter contained the collar thickness. Thus, the Reynolds number is

$$Re = \frac{G_m d_o}{\mu_b} \quad (5)$$

where $G_m = M/A_{min}$. In Equation (4), as suggested by McQuiston⁶, the flow geometry effects are represented by the exchanger finning factor

$$\epsilon = \frac{A_o}{A_{to}} \quad (6)$$

Combining the definition of the Stanton number and the sensible Colburn j -factor yields

$$j = \frac{Nu}{Re Pr^{1/3}} \quad (7)$$

Hence, it is apparent from Equation (4) that

$$j = C Re^{m-1} \epsilon^n \quad (8)$$

A multiple linear regression analysis of the experimental data permits the determination of the coefficients of Equation (8).

Determination of h_o , however, is made by first determining an overall heat transfer coefficient from the relationship

$$Q = U A F \Delta T_m \quad (9)$$

where ΔT_m = logarithmic mean temperature difference calculated by the measured inlet and outlet water and air temperatures and F = correction factor to the mean temperature difference¹¹. The overall heat transfer coefficient is related to the desired air-side film coefficient by

$$\frac{1}{U_o} = \frac{A_o}{A_i} \cdot \frac{1}{h_i} + \frac{1}{\eta_o} \cdot \frac{1}{h_o} + R_c \quad (10)$$

where R_c is the combined resistance of the tube wall and the collar. As this has a value of $3.8 \times 10^{-5} \text{ m}^2 \text{ }^\circ\text{C W}^{-1}$, it was neglected compared to the other terms of Equation (10).

The surface efficiency, η_o , is given by

$$\eta_o = 1 - \frac{A_f}{A_o} (1 - \eta_f) \quad (11)$$

Here, η_f , is the fin efficiency and is calculated as in Ref.13.

Due to the existence of fully developed turbulent flow inside the tubes, the water film coefficients, h_i , were determined by the Dittus–Boelter correlation¹⁴:

$$Nu_i = 0.023 Re_i^{0.8} Pr^{0.4} \quad (12)$$

Since the surface efficiency, η_o , depends upon h_o , an iterative determination of h_o from measured data was required.

Results and discussion

Preliminary heat transfer measurements were undertaken to check out the instrumentation and the methodology used in this study. There are a number of finned-tube configurations for which the experimental data are made available and can provide a basis for comparison with the results reported here. The related geometrical properties of the compared coils are presented in *Table 3*. The compared sensible heat transfer coefficients are given in *Figures 5–9*, and are consistent with the literature values. The coil hydraulic diameter, as defined by Equation (A13) in Appendix A, is used in determining the Reynolds numbers.

In general, the trends for the Colburn j -factors are in agreement with those documented in the literature. In *Figure 6*, due to experimental uncertainties at low flow rates, a maximum of 25% deviation in the results is noted. As the Reynolds number increases however the

Table 3 Geometric properties of the compared coils
Tableau 3 Propriétés géométriques des batteries comparées

Figure number	Reference	Finning factor ϵ	Hydraulic diameter d_h (mm)	Free flow area ratio σ
5	This study [12]	11.28	3.8	0.571
		11.23	3.9	0.579
6	This study [12]	14.43	3.0	0.560
		13.88	3.1	0.572
7	This study [3]	16.44	2.6	0.553
		17.54	2.7	0.543
8	This study [3]	15.81	3.8	0.546
		12.34	3.9	0.555
9	This study [5]	23.24	2.6	0.529
		21.41	2.7	0.540

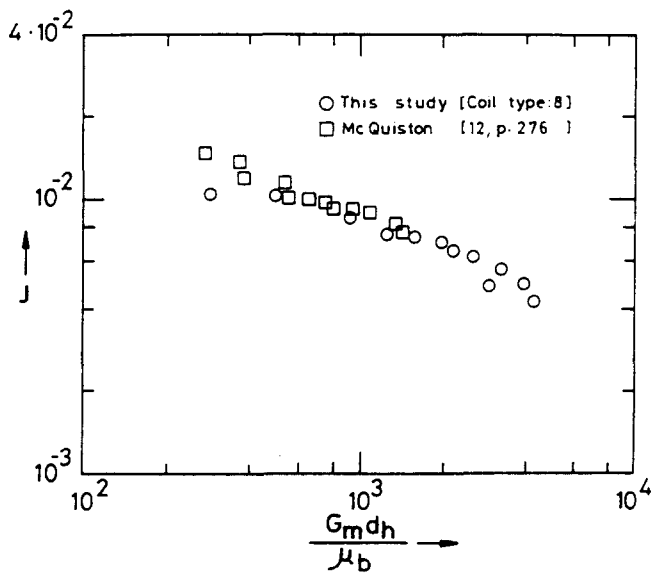


Figure 5 j versus Re_h : comparison of present heat transfer results with the data of McQuiston, $\epsilon = 11.28$
Figure 5 j par rapport à Re_h : comparaison des valeurs obtenues pour le transfert de chaleur avec les données de McQuiston, $\epsilon = 11.28$

discrepancy decreases. A similar trend is also observed in *Figure 8*. In this figure, the distinct behaviour of the two compared coils is attributed to 22% discrepancy in the finning factors. As given by Equation (8), the finning factor, ϵ , representing the surface geometry, directly influences the j -factor, and such deviations as in *Figure 8* are expected to occur. In *Figure 9*, while the proper trend is exhibited, Elmahdy's correlation for his test heater consistently shows higher values for the heat transfer. As illustrated in *Figure 5* of Ref. 5, Elmahdy reported an overestimation to data. Besides, the coil tested by Elmahdy contained eight rows in the flow direction. Then the higher j -factors in his work are also consistent with the conclusions of Rich⁴.

Reducing the measured values for a total of 110 experimental runs to j -factors as defined by Equation (7), all the data points are shown in *Figure 10*. The mean line through the 10 geometrical combinations of ϵ was obtained by a least-squares curve fit. In the least-squares treatment, the data points with Reynolds numbers below

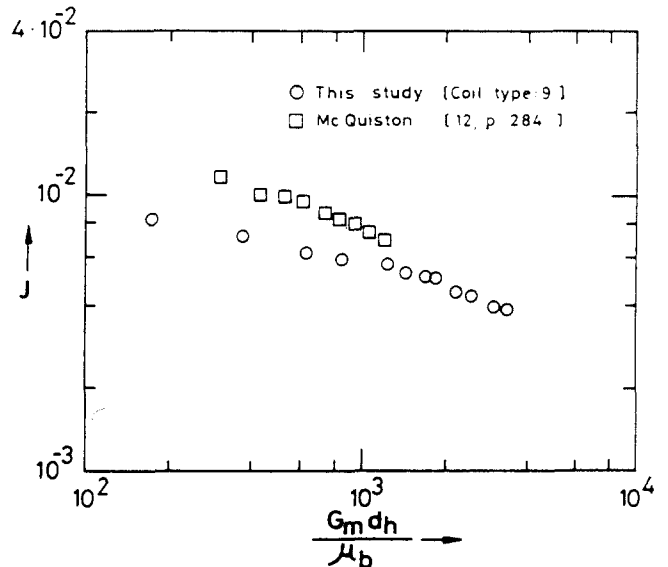


Figure 6 j versus Re_h : comparison of present heat transfer results with the data of McQuiston, $\epsilon = 14.43$
Figure 6 j par rapport à Re_h : comparaison des valeurs obtenues pour le transfert de chaleur avec les données de McQuiston, $\epsilon = 14.43$

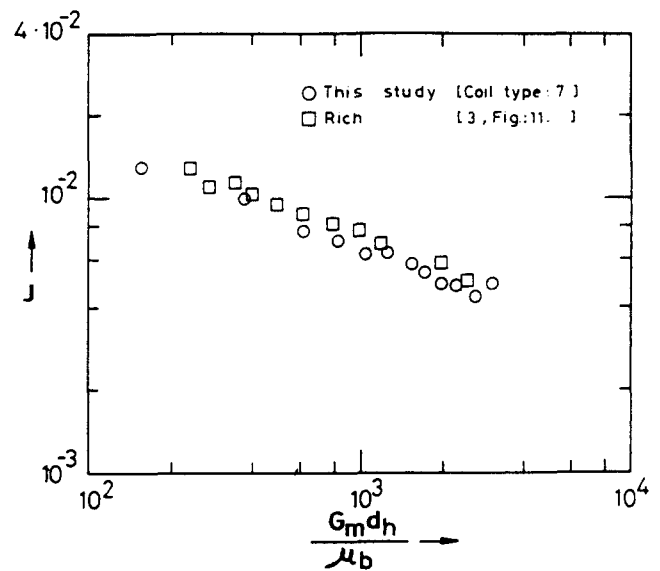


Figure 7 j versus Re_h : comparison of present heat transfer results with the data of Rich, $\epsilon = 16.44$
Figure 7 j par rapport à Re_h : comparaison des valeurs obtenues pour le transfert de chaleur avec les données de Rich, $\epsilon = 16.44$

500 were excluded because of the low Reynolds number effects – conduction and natural convection – which preclude a boundary type of analysis. Accordingly the following correlation is determined:

$$j = 0.15 Re^{-0.28} \epsilon^{-0.362} \tag{13}$$

in which $500 < Re < 30\,000$ and $11.2 \leq \epsilon \leq 23.5$.

The thermophysical properties in Equation (13) are evaluated at the arithmetic average of the air inlet and outlet bulk temperatures.

A search of the literature revealed that attempts have

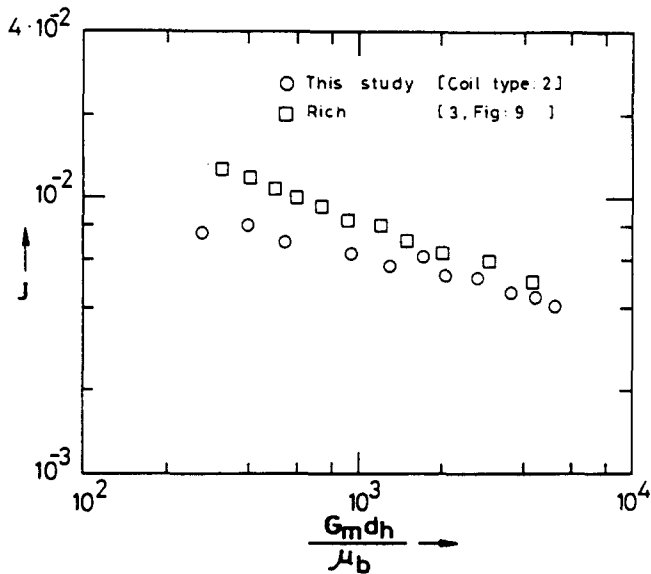


Figure 8 j versus Re_b : comparison of present heat transfer results with the data of Rich, $\epsilon = 15.81$
 Figure 8 j par rapport à Re_b : comparaison des valeurs obtenues pour le transfert de chaleur avec les données de Rich, $\epsilon = 15,81$

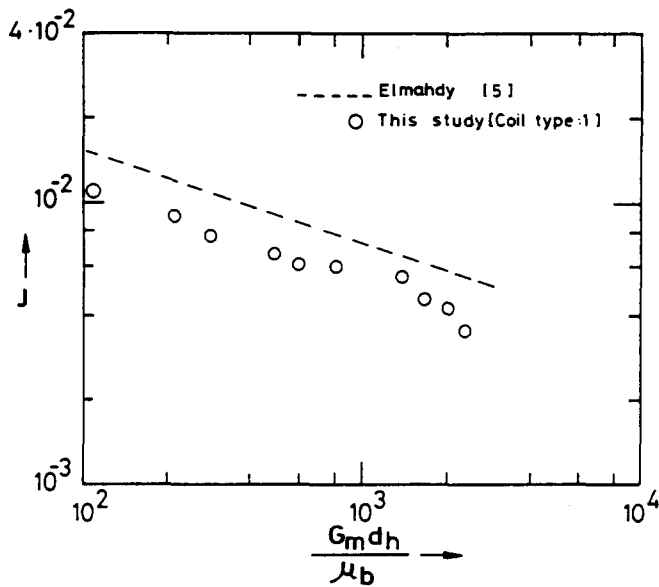


Figure 9 j versus Re_b : comparison of present heat transfer results with Elmahdy's correlation, $\epsilon = 23.24$
 Figure 9 j par rapport à Re_b : comparaison des résultats actuels du transfert de chaleur avec la corrélation de Elmahdy, $\epsilon = 23,24$

been made to obtain generalized correlations for the heat transfer coefficients related to the subject of the present study by McQuiston⁶ and recently by Webb¹⁵. In McQuiston's analysis, however, the channel effect of the fins was neglected, and the flows over the finned tube surface and over the bank of bare tubes were assumed to be similar. Then, for Reynolds number in the range of 100 to 4000, the exponent $m - 1$ of Equation (8) was -0.4 .¹⁴ Due to the presence of fins, the flow along the flat plate is superimposed on the flow around the tubes. The fin effect becomes stronger especially at high Reynolds numbers. Hence the exponent $m - 1$ should assume a value between -0.4 and -0.2 in which the lower limit

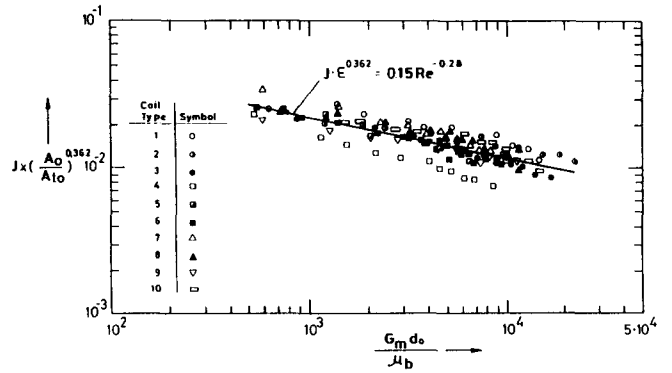


Figure 10 Average convective heat transfer as a function of Reynolds number, $11.2 < \epsilon < 23.5$
 Figure 10 Transfert de chaleur par convection moyen en fonction du nombre de Reynolds, 11,2

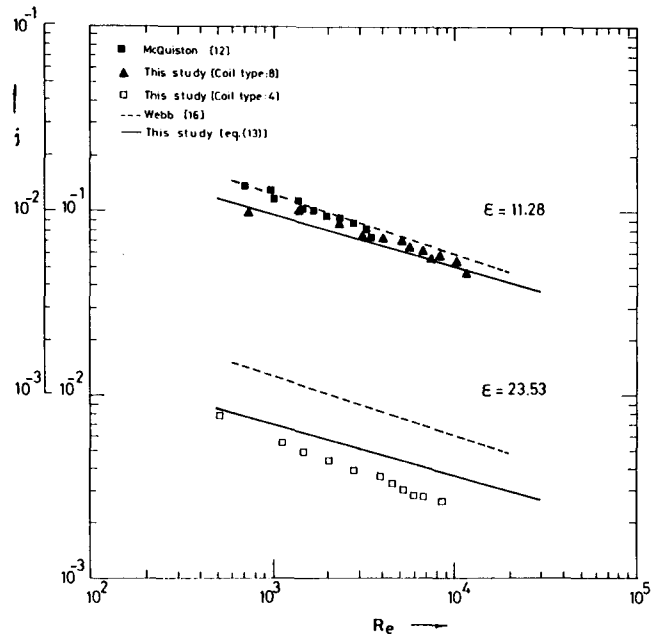


Figure 11 Including the data for coil types 8, 4, and McQuiston¹², comparison of the present correlation with Ref. 16
 Figure 11 Position des données concernant les batteries 8 et 4 et des résultats de McQuiston¹² dans le diagramme de la corrélation utilisée et de la réf. 16

represents the tube bank and the upper limit the channel flows. Implementing a multiple regression technique to the data of 16 flat-plate heat exchangers, Gray and Webb¹⁶ developed a correlation in which the Reynolds number exponent was -0.328 . In this study, the j -factor slope is determined to be -0.28 . Such a slope value appears to be in agreement with the strong channel effect of fins on the flow at high Reynolds numbers. Elmahdy⁵ reported slopes ranging from -0.36 to -0.30 for several geometrically different exchangers. The slope discrepancy may be due to the distinct definition of characteristic length in Elmahdy's work.

The present data for coil types 8 and 4 are compared with the correlation stated by Webb (Equation (5) in Ref. 16) in Figure 11. Starting from the first distribution for $\epsilon = 11.28$ which also contains the data of McQuiston¹²,

it should be noted that Webb's correlation represents the results with reasonable accuracy at low Reynolds numbers. As the Reynolds number increases, however, the correlation line diverges from the data points. Defining the percentage of error in the j -factor representation as

$$E = \frac{(j_{\text{analytical}} - j_{\text{experimental}})}{j_{\text{analytical}}} \times 100 \quad (14)$$

where $j_{\text{analytical}}$ is the j -factor calculated by using any of the stated correlations, then, typically at $Re = 12\,000$, Webb's correlation is found to deviate by 29.5% while Equation (13) deviates by 8.2%. In the second distribution for $\epsilon = 23.53$, the geometric ratios for coil type 4 are $s_1/d_o = 3.02$ and $s_2/d_o = 2.62$, and exceed the range of validity of Webb's correlation. As shown in the figure, Webb's correlation exhibits a large discrepancy with the present data. It is quite difficult to interpret this particular manifestation. However, as noted by Webb¹⁶, the small influence of fin spacing, especially at high flow rates, is probably misleading. Considering a limit case for which s_1/d_o and s_2/d_o are assumed to possess large values and $s/d_o \ll 1$, then it would not be appropriate to neglect the channel effect of fins on the flow and disregarding this effect may lead to higher j -factors. In Figure 11, at $Re = 9000$, Equation (13) displays a maximum of 31% error to the data for coil type 4.

Practical significance

The results of this study represent the first phase of a research programme motivated by the need to develop an improved understanding and characterization of forced convection heat transfer on compact plate-fin heat exchanger surfaces. In addition, to confine variations in the exchanger surface geometry, existing correlations in the engineering literature are only applicable to a limited range of Reynolds numbers. However, heat exchanger designers and analysts require a correlation, with reasonable accuracy, validated for a wide span of Reynolds numbers and for diversified geometrical conditions. The present study aims to fulfil this requirement. The exchanger finning factor obtained by means of Equation (A10) can be applied in Equation (13) to predict the performance characteristics of untested but geometrically similar heat exchangers, provided they are operated in the Reynolds number range 500 to 30 000.

Conclusion

In the experiments, the geometrical parameters of the 10 tested coils were varied in the ranges of $2.39 < s_1/d_o < 3.15$, $2.07 < s_2/d_o < 2.67$, and $0.131 < s/d_o < 0.425$. Containing the collar thickness, the Reynolds number presentation is based on the tube outside diameter. As described in the Appendix, all the geometrical properties are embodied in a single parameter: the finning factor, ϵ . The performance of a plate finned tube heat exchanger is best expressed in terms of a Colburn j -factor and a relation between this and the Reynolds number, the finning factor, is then sought.

A strong dependence of the heat transfer coefficients on the finning factor, ϵ , is noted. As the value of ϵ increases, the general behaviour of the exchanger, as

expected, is a decrease in the j -factor. By Equation (A10), the fin density, s_F , being a major parameter in ϵ representation, the more dense the fins are, the more the channel effect is pronounced.

Although Equation (13) represents the data points with a correlation coefficient of 0.93, care should be exercised in using the results. The 71.8% of all the data in Figure 10 are determined to lie in a $\pm 10\%$ dispersion band around the mean line. Out of 110 experimental data, however, 5 and 14 data points are found to scatter respectively by $+30$ and -30 deviations which also indicates the upper and the lower limits of error for Equation (13).

Acknowledgement

The work reported is part of a research project sponsored by Turbo-Therm Heat Exchangers Manufacturing Corporation. Their financial and technical support is gratefully acknowledged.

References

- 1 Webb, R.L. Air-side heat transfer in finned tube heat exchangers *Heat Transfer Eng* (1980) 1 (3) 33–49
- 2 McQuiston, F.C. Finned tube heat exchangers: state of the art for the air side *ASHRAE Trans* (1981) 87 1077–1085
- 3 Rich, D.G. The effect of fin spacing on the heat transfer and friction performance of multi-row, smooth plate fin-and-tube heat exchangers *ASHRAE Trans* (1973) 79 (part 2) 137–145
- 4 Rich, D.G. The effect of the number of tube rows on heat transfer performance of smooth plate fin-and-tube heat exchangers *ASHRAE Trans* (1975) 81 (part 1) 307–317
- 5 Elmahdy, A.H., Biggs, R.C. Finned tube heat exchanger: correlation of dry surface heat transfer data *ASHRAE Trans* (1979) 85 (part 2) 262–273
- 6 McQuiston, F.C. Correlation of heat, mass and momentum transport coefficients for plate-fin-tube heat transfer surfaces with staggered tubes *ASHRAE Trans* (1978) 84 (part 1) 294–309
- 7 Kays, W.M., London, A.L. Heat transfer and flow friction characteristics of some compact heat exchanger surfaces – Part 1: Test system and procedure *Trans ASME* (1950) 72 1075–1085
- 8 British Standard BS 1042 (part 2A) (1973) 38–59
- 9 Kline, S.J., McClintock, F.A. Describing uncertainties in single-sample experiments *Mech Eng* (1953) 75 3–8
- 10 Colburn, A.P. A method of correlating forced convection heat transfer data and a comparison with fluid friction *Trans AICHE* (1933) 29 174–210
- 11 VDI-Wärmeatlas Berechnungsblätter für den Wärmeübergang, VDI-Verlag GmbH (1963)
- 12 McQuiston, F.C. Heat, mass, and momentum transfer data for five plate-fin-tube heat transfer surfaces *ASHRAE Trans* (1978) 84 (part 1) 266–293
- 13 McQuiston, F.C., Parker, J.D. *Heating, Ventilating, and Air Conditioning – Analysis and Design* 3rd Edn, John Wiley, New York, (1988) 555–562
- 14 Incropera, F.P., Dewitt, D.P. *Fundamentals of Heat and Mass Transfer* 2nd Edn, John Wiley, New York, 1985, pp. 309–404
- 15 Webb, R.L. Enhancement of single-phase heat transfer Chapter 17 In *Handbook of Single-Phase Convective Heat Transfer* S. Kakaç, R.K. Shah, W. Aung, (eds) John Wiley, Chichester (1987) 17.16–17.17
- 16 Gray, D.L., Webb, R.L. Heat transfer and friction correlations for plate finned-tube heat exchangers having plain fins *Proceedings of 8th Int Heat Transfer Conference* (1986) 6 2745–2750

Appendix

Heat exchanger geometry

In order to relate the finning factor to the geometry of the heat exchanger, it is necessary to consider the follow-

ing definitions for the plate-fin, cross flow, staggered-tube exchanger. Referring to *Figure 2*, denoting the tube outside diameter by d_o and the collar thickness by t_c , then the characteristic dimension becomes:

$$d_o = d_{to} + 2t_c \quad (A1)$$

The relation between the number of tubes per row, n , the transverse pitch, s_1 , and the exchanger height, B , is:

$$B = n \cdot s_1 \quad (A2)$$

Similarly, the number of the tube rows, N , the longitudinal tube pitch, s_2 , and the flow length, L , are related as:

$$L = N \cdot s_2 \quad (A3)$$

Then the minimum flow area per unit length and the exchanger frontal area per unit length are:

$$A_{min} = n(s_1 - d_o) (1 - t_{sF}) \quad (A4)$$

$$A_{fr} = n \cdot s_1 \quad (A5)$$

The parameter, s_F , is termed the fin density and has units of fins per unit length. The ratio of Equations (A4) and (A5) becomes:

$$\sigma = \left(1 - \frac{d_o}{s_1}\right) (1 - t_{sF}) \quad (A6)$$

The finned area per unit length and the tube outside area with collar per unit length are given by

$$A_f = Nn \frac{\pi d_o^2}{2} \left[\frac{4}{\pi} \cdot \frac{s_1}{d_o} \cdot \frac{s_2}{d_o} - 1 \right] s_F \quad (A7)$$

$$A_{to} = Nn\pi d_o (1 - t_{sF}) \quad (A8)$$

Then, the total outside surface area per unit length is:

$$A_o = Nn\pi d_o \left[\left(1 - t_{sF}\right) + \frac{d_o}{2} \left(\frac{4}{\pi} \cdot \frac{s_1}{d_o} \cdot \frac{s_2}{d_o} - 1 \right) s_F \right] \quad (A9)$$

Together with Equations (A9), (A8), and (A6), the definition of the finning factor, ϵ , yields:

$$\epsilon = 1 + \left(\frac{4}{\pi} \cdot \frac{s_1}{d_o} \cdot \frac{s_2}{d_o} - 1 \right) \left(1 - \frac{d_o}{s_1} \right) \frac{d_o s_F}{2\sigma} \quad (A10)$$

Furthermore, the total inside area of the coil tubes per unit length is as follows:

$$A_i = Nn\pi d_i \quad (A11)$$

Having thus described the characteristic geometry of the heat exchanger, it is apparent that the hydraulic diameter is defined as:

$$d_h = \frac{4\sigma A_{fr} L}{A_o} \quad (A12)$$

In terms of the geometrical properties of the exchanger, the following relation for the hydraulic diameter may be derived:

$$d_h = \frac{8\sigma}{\pi} \cdot \frac{(s_1/d_o) (s_2/d_o)}{\frac{2}{d_o} (1 - t_{sF}) + \left(\frac{4}{\pi} \cdot \frac{s_1}{d_o} \cdot \frac{s_2}{d_o} - 1 \right) s_F} \quad (A13)$$